Biophysical Journal Volume 103 August 2012 601–609

High Density Waves of the Bacterium *Pseudomonas aeruginosa* in Propagating Swarms Result in Efficient Colonization of Surfaces

Huijing Du,[†] Zhiliang Xu,[†] Morgen Anyan,[‡] Oleg Kim,[†] W. Matthew Leevy,[§¶] Joshua D. Shrout,[‡||**] and Mark Alber[†††*]

[†]Department of Applied and Computational Mathematics and Statistics, [‡]Department of Civil Engineering and Geological Sciences, [§]Notre Dame Integrated Imaging Facility, [¶]Department of Chemistry and Biochemistry, [||]Department of Biological Sciences, and **Eck Institute for Global Health, University of Notre Dame, Notre Dame, Indiana; and [††]Department of Medicine, Indiana University School of Medicine, Indiana

ABSTRACT This work describes a new, to our knowledge, strategy of efficient colonization and community development where bacteria substantially alter their physical environment. Many bacteria move in groups, in a mode described as swarming, to colonize surfaces and form biofilms to survive external stresses, including exposure to antibiotics. One such bacterium is *Pseudomonas aeruginosa*, which is an opportunistic pathogen responsible for both acute and persistent infections in susceptible individuals, as exampled by those for burn victims and people with cystic fibrosis. *Pseudomonas aeruginosa* often, but not always, forms branched tendril patterns during swarming; this phenomena occurs only when bacteria produce rhamnolipid, which is regulated by population-dependent signaling called quorum sensing. The experimental results of this work show that *P. aeruginosa* cells propagate as high density waves that move symmetrically as rings within swarms toward the extending tendrils. Biologically justified cell-based multiscale model simulations suggest a mechanism of wave propagation as well as a branched tendril formation at the edge of the population that depends upon competition between the changing viscosity of the bacterial liquid suspension and the liquid film boundary expansion caused by Marangoni forces. Therefore, *P. aeruginosa* efficiently colonizes surfaces by controlling the physical forces responsible for expansion of thin liquid film and by propagating toward the tendril tips. The model predictions of wave speed and swarm expansion rate as well as cell alignment in tendrils were confirmed experimentally. The study results suggest that *P. aeruginosa* responds to environmental cues on a very short timescale by actively exploiting local physical phenomena to develop communities and efficiently colonize new surfaces.

INTRODUCTION

Bacterial biofilms are structured cellular communities that represent the dominant bacterial growth state for both environmental and clinical scenarios. There is great interest to understand biofilm assembly, as infections resulting from biofilms are notoriously resistant to antibiotic treatments. Treatment of a broad spectrum of human health issues, ranging from lethal infections from opportunistic pathogens such as those in cystic fibrosis patients, to catastrophic failure of prosthetic implants, could improve with a greater understanding of biofilm formation. Among the biofilm development steps for which we lack understanding is the ability of bacteria to first colonize host surfaces.

Bacterial swarming motility has been shown to be important to biofilm formation (1–3), where cells act not as individuals, but as coordinated groups to move across surfaces, often within a thin-liquid film (4–6). It has been suggested that bacterial swarms are sufficiently cooperative that noncontributing cheaters cannot survive in swarms (7,8). Many swarming bacteria are aided by the production of a surfactant that lowers surface tension of the liquid film to improve bacterial motility (6). The components of cell motion during swarming are currently best described for *Escherichia coli* and *Paenibacillus* spp., which spread as monolayers of motile cells (9–14).

For *Pseudomonas aeruginosa*, which does not swarm as a monolayer, the cell and fluid patterns are difficult to discern using current experimental methods. It is not yet known if swarming *P. aeruginosa* cells behave solely as swimming cells (15), or if twitching, sliding, or walking motility (16–19) are also important to swarming. These swarming communities of *P. aeruginosa* represent a complex intersection of physical, biological, and chemical phenomena. The branched tendril patterns that are often, but not always, observed in *P. aeruginosa* swarms (8,20) require production of rhamnolipid (RL) (21,22). RL is an extracellular lipid that acts as a surfactant to reduce surface tension in bacterial suspensions. RL production by *P. aeruginosa* is not constant and is regulated by intercellular quorum sensing (QS) signaling. RL synthesis is only initiated when a sufficient, actively growing QS signal-producing population is present (23,24). In addition to RL, a functional bacterial flagellum is also required for swarms to form tendrils (20,21).

Some barriers to better understanding collective behaviors within swarming groups have been overcome by using computer simulations. For example, one-dimensional models have been used to describe biological and hydrodynamic aspects of *Serratia liquefaciens* swarm expansion (25,26)

Submitted March 12, 2012, and accepted for publication June 19, 2012.

*Correspondence: albemark@gmail.com

Editor: Richard Bertram.

0006-3495/12/08/0601/9 $2.00

http://dx.doi.org/10.1016/j.bpj.2012.06.035

and surfactant-mediated spreading (against gravity, up a glass surface) of *Bacillus subtilis* (27). A cell-based stochastic modeling approach was used to study the role of reversals, cell bending, and cell-slime interactions during swarming of *Myxococcus xanthus* (28–30). A recent multiscale three-dimensional computational model of *P. aeruginosa* swarming (31) couples continuous submodels for describing fluid dynamics (similar to the one in (25–27)) and chemical signal propagation with a stochastic discrete submodel for simulating individual cells and their surfactant production within the swarm.

In this work, we investigate a novel, to our knowledge, biological phenomenon in which we observed the development and propagation of cell waves and formation of branched tendril patterns controlled by bacterial population and self-production of RL. This population-dependent production of RL results in an osmotically driven extraction of water and a Marangoni-driven expansion of the liquid film at the edge of the bacterial colony. Here we show, for the first time, to our knowledge, the spatiotemporal localization of bacteria and RL during *P. aeruginosa* swarming. We first describe in this work our experimental results that demonstrate formation and propagation of bacterial and RL waves during *P. aeruginosa* swarming. We also show that cell density increases exponentially in front of the internal wave close to the swarm edge.

We then employ simulations using a biologically justified cell-based multiscale model to hypothesize mechanisms leading to wave propagation and branched tendril formation. We propose that cell wave propagation is due to a combination of increased cell division, RL production, and cell-cell alignment when cells leave the initial inoculation region. Subsequent tendril formation would depend upon competition between the changing viscosity of the bacterial liquid suspension and the liquid film boundary expansion caused by Marangoni forces. We show that *P. aeruginosa* branched tendril formation is different from the purely liquid film phenomenon observed earlier in many physical systems (32–37). Simulations suggest that *P. aeruginosa* cells align to facilitate their swarm expansion. This is confirmed by analyzing images of the swarm obtained experimentally. Analysis of the combined experimental and simulation results suggest that the directed motion of cell waves into tendrils provides a highly efficient strategy to colonize surfaces. Furthermore, the multibranched (fractal) structure of the swarm edge increases its length providing efficient packaging, and optimizes bacterial access to oxygen and other nutrients.

The layout of the work is as follows. It starts with the Materials and Methods section, followed by detailed descriptions of the multiscale model in the Multiscale Model section. Discussion of the combined experimental and simulation results is presented in the Results, and the article ends with the Conclusions.

MATERIALS AND METHODS

Experimental techniques

P. aeruginosa swarming of GFP-tagged cells was examined using plate assays solidified with soft (0.45%) noble agar amended with the lipid stain Nile Red as a visual indicator of spatial RL distribution and were imaged over time (38). Swarm assay plates were inoculated with log-phase cells ($OD_{600} \approx 0.7$).

Imaging techniques

Whole-plate fluorescence images of swarm plates were acquired using a Carestream Multispectral FX imaging station (Carestream Health, Woodbridge, CT) (38). Excitation and emission wavelengths for GFP and Nile Red were 480/535 and 540/600 nm, respectively. Additional images were acquired at high resolution: horizontal scans were taken every millimeter between the center of the swarm and the end of multiple tendrils using the z-stack function of a Nikon A1 confocal microscope. Individual images were taken every half micrometer between the top and bottom of the swarm, and then assembled into a single three-dimensional image of the swarm. Images were further processed using Nikon Elements software.

Multiscale model

In this section, we describe the multiscale model of *P. aeruginosa* swarming. (Complete description of the model can be found in (31).) To summarize, the off-lattice stochastic cell model introduced in (28,29), is used to simulate individual *P. aeruginosa* cell growth, deformation, cell-cell alignment, as well as motion in fluid described by the thin film continuous submodel. Cell growth depends on the local nutrient concentration. A simplified QS cell submodel involves one QS signal molecule (corresponding to *n*-acylhomoserine lactone), which activates the synthesis of RL. If the concentration of RL is greater than a given threshold, liquid is extracted from the substrate. Cells can be in the solitary or activated state depending on the QS concentration. Propagations of the QS signal and RL at the macroscale are modeled using convection-diffusion-reaction equations.

Off-lattice stochastic cell submodel

Individual *P. aeruginosa* cells are represented by a set of elastically connected nodes (similar to (28,29), see Fig. 1 *A*). The nodes are classified as head node, body node, and tail node. Nodes are connected by the line segment. The width d of each segment is $d = 2R$ and its length is l_i. Here, L_c is half of the average cell length measured in experiment and R is the average radius of the cell. The neighboring segments form angles θ_i. For each cell we define a cell-body-configuration energy (Hamiltonian) H, which consists of stretching and bending terms:

$$H = \sum_{i=1}^{N-1} K_b (l_i - L_c)^2 + \sum_{i=1}^{N-2} K_\theta \theta_i^2. \quad (1)$$

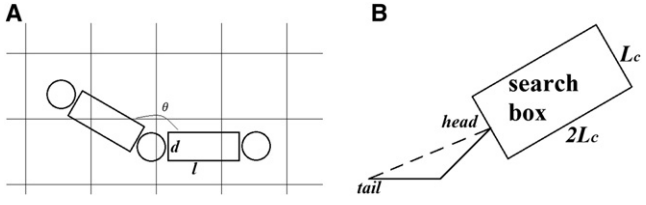

FIGURE 1 (*A*) Schematic diagram of a cell representation with three nodes connected together characterized by basic parameters. (*B*) Cell search box of a cell to make cell-cell alignment.

Here, K_b and K_θ are stretching and bending coefficients, analogous to the spring constants in Hooke's Law. N is the number of nodes used to represent a cell. To move a cell, first, the position of the cell head node is updated based on its current velocity calculated using biological rules determined by the local environment. If the liquid depth is >10 μm (~10 times of the cell width), cells swarm within liquid using flagella and align with each other; otherwise, cells just move randomly. We model cells aligning with each other based on previously justified local rules for bacteria (28,29) (see Fig. 1 *B*). Namely, we average the orientation of neighboring cells for a given cell within a rectangular domain of size $2\ L_c \times L_c$, where L_c is half of the average cell length. Assuming the height of the liquid film at the location of the cell being >10 μm, the direction of the head node movement is chosen as a linear combination (with 0.1, 0.45, and 0.45 as coefficients) of a random walk direction, direction of the liquid film movement at the cell location, and the averaged direction of its neighboring cells.

After updating the position of the head node of a cell, positions of the body and tail nodes are adjusted using the Monte Carlo algorithm (28,29,31). Body and tail nodes of the cell are capable of making a number of tentative movements. The tail node tends to move along the direction pointing from itself to the middle node, whereas the middle node moves in the direction from tail to the head node. Each tentative movement is accepted with probability P determined by $\Delta H = H_1 - H_0$, the change of the cell-body-configuration energy (Eq. 1), using the Metropolis Monte Carlo algorithm (39):

$$P = 1 \text{ if } \Delta H \leq 0;\ P = \exp\left(-\frac{\Delta H}{kT}\right) \text{ if } \Delta H > 0, \quad (2)$$

where k is the Boltzmann constant and T is a parameter that characterizes the cell's body tendency to fluctuate from the equilibrium. H_1 is the cell-body-configuration energy calculated for a specific tentative movement, whereas H_0 is the energy of the previous movement. If ΔH is <0, this tentative movement is accepted and the cell moves to a new position; if ΔH is >0, this new movement is accepted with a probability $\exp(-\Delta H/kT)$. Namely, if a randomly generated number is less than $\exp(-\Delta H/kT)$, the tentative movement is accepted, otherwise the cell does not move. (Each cell in the model is capable of making 15 tentative movements per time step balancing cell flexibility and computational cost.) Stochastic features of the cell body movement enable a cell to keep its length and level of bending within certain ranges. Table 1 lists parameter values used in the stochastic cell submodel.

The model also incorporates cell growth and division. Growing and moving cells consume nutrient. As the nutrient level in a cell reaches a threshold, the cell divides into two daughter cells. This threshold value is determined from the experimentally observed *P. aeruginosa* population doubling time (over a period of 1 h). For simplicity, individual cells are assumed to always maintain a level of QS signal, which enables them to secrete the signal to the environment (40), increasing the QS concentration at the cell location. Once it is greater than the given threshold, cells within this region are activated from the solitary state to begin production and release of RL. If the concentration of RL is greater than a given threshold, water is extracted from the substrate. (See the Supporting Material for more details.) Although more simplified than the dual QS signal approach employed by others (41,42), this simplified model does enable us to capture the key phenomena of *P. aeruginosa* swarming. A more detailed QS submodel will be included in future simulations.

TABLE 1 Parameters for off-lattice stochastic cell submodel

Parameters	Values	Reference
Number of nodes per cell (N)	$N = 3$	(28,29)
Cell width; cell length	$0.3 - 0.8$ μm; $1.0 - 1.2$ μm	
Stretching coefficient (K_b); bending coefficient(K_θ)	$5\ Emicron^{-2}$; $2\ E$	(28,29)
Boltzmann constant times temperature (kT)	$2\ E$	(28,29)
Individual cell velocity	4.64 cell length min^{-1}	(3)

The following initial conditions are implemented in the simulations. Nutrient is assumed to be abundant; therefore, stationary or starvation states are not considered in this work. The QS chemical concentration is set to be low, and all cells are assumed to be in the solitary or planktonic state in the start of each simulation.

Continuous submodels

The depth of a typical colony is much smaller than its extent. Therefore, we employ the following thin viscous liquid film equation (26,43) to describe the liquid layer:

$$h_t = -\nabla\cdot\left(h\left(\frac{\gamma_m}{3\mu}h^2\nabla\nabla^2 h + \frac{h}{2\mu}\nabla\gamma\right)\right) + Eh. \quad (3)$$

Here, h is the thickness of the liquid film. Surface tension γ depends on the RL concentration Γ. E represents the rate of extracting water from the substrate by osmotic effects of RL and is proportional to the local RL concentration. We use the following constitutive law (34,37,43) to describe the dependence of the surface tension on the surfactant RL concentration:

$$\frac{\gamma}{S} = (\alpha+1)\left(1 - \frac{\Gamma}{\Gamma_m}\left[\left(\frac{\alpha+1}{\alpha}\right)^{1/3} - 1\right]\right)^{-3}, \quad (4)$$

where $\alpha = \gamma_m/S$. Viscosity μ is dependent on the density of the suspension of cells. We also adopt the following effective Newtonian viscosity model (25,26,44):

$$\frac{\mu}{\mu_0} = \chi(\phi)\left[1 + \frac{1.44\phi^2\chi(\phi)^2}{1 - 0.1241\phi + 10.46\phi^2}\right], \quad (5)$$

where

$$\chi(\phi) = \frac{1 - 0.5\phi}{(1-\phi)^3}. \quad (6)$$

Here, ϕ is the volume density of cells and μ_0 is the pure solvent viscosity. *P. aeruginosa* cells secrete soluble RL, which changes the surface tension of the liquid film. Marangoni stresses arise due to nonuniformities in the surface tension at the interface between the gaseous and aqueous phases that are induced by the local differences in interfacial surfactant concentration. These stresses drive flow from areas of high surfactant concentration to lower surfactant regions. The term $\nabla\cdot(h^2/2\mu\ \nabla\gamma)$ accounts for the Marangoni-driven instability. Macroscale evolutions of nutrient, QS signal, and RL are modeled using convection-diffusion reaction equations (31).

Integration of the submodels into a multiscale model

First, the off-lattice cell submodel is solved to update positions of bacterial cells, and liquid depth at the location of each cell is calculated by interpolating h, the thickness of the liquid film from the partial differential equation (PDE) grid. Cell-environment interactions are then simulated. Each cell consumes a certain amount of nutrient represented by a source term in the convection-diffusion equation (see (31) for details). Production of the QS signal and RL, and their release to the environment by cells, are then

implemented. Bacterial cell density is computed on each PDE grid block. An interpolation operator is used to distribute cell produced RL to PDE grid blocks. Next, effective viscosity of the fluid at each grid cell is updated according to Eqs.5 and 6 based on the distribution of bacterial cells. Finally, convection-diffusion-reaction equations and the thin viscous liquid film Eq. 3 are solved to update chemical concentration and to evolve liquid film. The model parameter values are listed in Table 1 and Table S1.

RESULTS

By imaging the population density of the entire swarms (as in (38)) over time, we observed that cells in tendril-forming swarms of *P. aeruginosa* move in a high density wave (ring-like pattern) propagating radially toward branched tendril structures forming at the edge of the swarm on soft agar (0.45%) surfaces (Fig. 2). This results in accumulation of high density groups of cells close to the ends of these tendrils. We also observed that a RL-dense wave accompanies the cell-dense wave propagation. The RL distribution in these tendril swarms is also nonuniform but is less pronounced than the cell density distribution (*bottom row* of Fig. 2) because RL is soluble and more readily diffuses (compared to cells) within the liquid film.

We monitored the behavior of both tendril-forming swarms growing on soft agar and nontendril swarms growing on hard agar (0.6%) for comparison (20). As shown in Fig. 3 *A*, the temporal swarming profiles of both swarms can be separated into two phases. Phase I lasts for ~25 h and represents the lag (6) and acceleration of swarm colony growth. The expansion rate was 0.15 cm^2/h during this phase.

Phase II represents swarming after 25 h where the swarm colony size increases exponentially. Fig. 3 *B* shows the population dynamics of the swarm along the radial direction. The internal high density cell wave shown in Fig. 2 develops from the inoculation point and propagates outward along the radial direction as a ring (see Movie S1). The cell wave spreads faster than the advancing swarm edge. Assuming a power law of expansion, we calculated the swarming exponent, α, based upon the expression $r \propto t^{\alpha}$, where t is the time and r is the radial position of the wave or the swarm edge (45,46). For the swarm shown in Fig. 2, α values were 0.82 and 0.36 for the internal wave and the swarm edge, respectively (see Fig. 4 *A*).

Another substantial difference between liquid film physical phenomenon (32–37) and *P. aeruginosa* swarming is that suspended bacteria increase the effective viscosity of the liquid film and liquid movement slows due to increased viscosity (44). Moreover, RL, produced by *P. aeruginosa* swarming cells, can act osmotically as a solute (47) to extract water from the semisolid agar (48) and can decrease the surface tension of the liquid layer, which allows easier flagellar rotation within the liquid film (6,49–52). The overall effect of RL upon swarming is dramatic as the motion of wild-type bacterial swarm is strongly affected by fluid effects during tendril formation (see Movie S2) when compared with motility of a RL-deficient *P. aeruginosa* strain (see Movie S3). Therefore, we hypothesized that the mechanism of branched tendril formation was based upon the competition between constantly changing viscosity of the bacterial liquid film and liquid film boundary expansion caused by the Marangoni forces (32,36) due to changes in surface tension of the liquid film.

To test this hypothesis, we ran simulations using the multiscale model of *P. aeruginosa* swarming (31) which is described in the Multiscale model section. The initial and boundary conditions of simulations are given in the

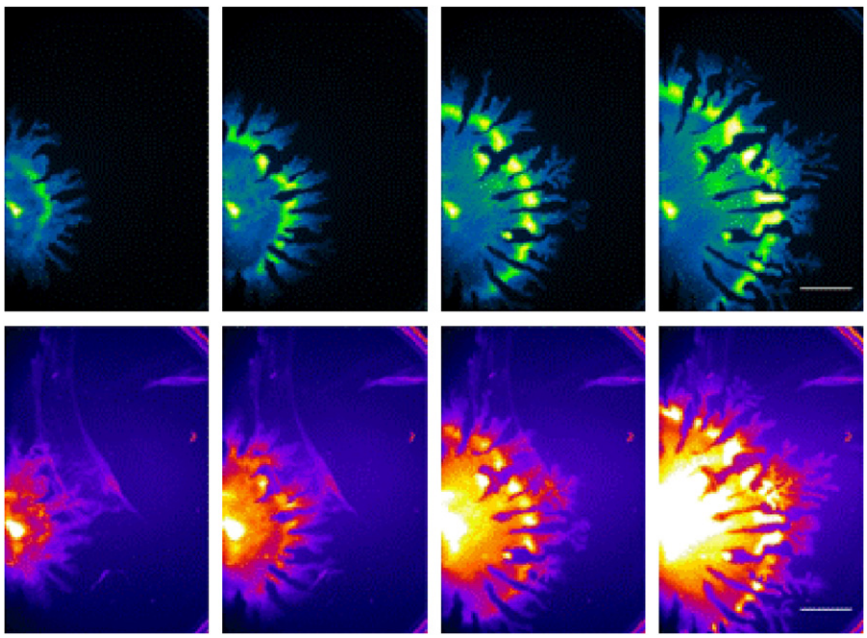

FIGURE 2 *Pseudomonas aeruginosa* swarming and RL concentration over time. Swarms on soft agar form tendrils when high concentrations of RL are present (snapshots taken from Movie S1). Both *P. aeruginosa* cell density (*blue-green*) and RL (*red-fire*) concentrations distribute as a wave (*white*) through the developing swarm. Images at 6-h intervals (from 12 to 30 h) are presented (Scale bar = 15 mm).

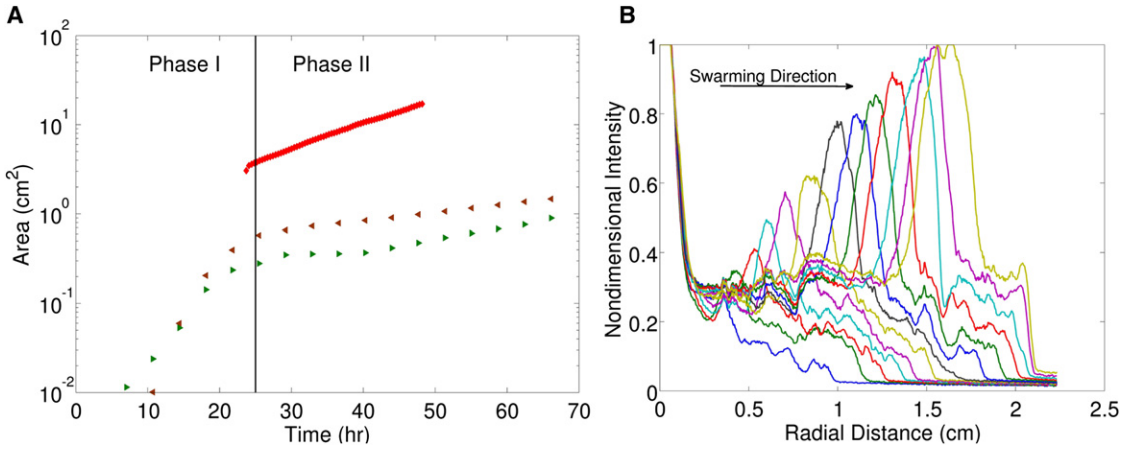

FIGURE 3 (*A*) Area of bacterial swarms as a function of time. Green and dark red triangles represent swarming on hard agar plates, and the red line represents swarming on soft agar plates (Movie S1). (*B*) Image intensity profiles of the swarming *P. aeruginosa* colony on soft agar as functions of the radial distance at time intervals of 111.25 min. Image intensity values were normalized with respect to the value at the center of the bacterial colony. Assuming that intensity is proportional to the bacterial density, the shown profiles demonstrate the dynamics of the cell density along the radial direction of the colony.

Supporting Material. Fig. 3 *B* shows that, in experiments, the cell density within the wave increases as the wave propagates radially. On the basis of these experimental observations, we assumed for our simulations, that after leaving the initial inoculation region, cells would increase their division and RL production rates by a factor of four. We also assumed that cells exhibit an alignment resulting in cell clusters. (Cell alignment was confirmed by examining bacteria present in the swarm tendrils under 100× magnification. See Fig. 5 and Experimental Results about Cell Alignment.) Our silico simulations indicate that cells quickly disperse outward as a wave in a ring pattern; this initial wave of cells forms as the cell-containing liquid film expands by Marangoni forces. Subsequently, the cell wave is maintained over time due to the increased rates of cell division and RL production (see discussion below, without increased rates of cell division and RL production, simulations did not produce the cell wave). The simulations suggest that the tendril patterns observed on soft agar could be induced by a liquid film instability initiated at the edge of the swarm. Fig. 6 shows both simulated and experimental swarm edge regions to detail the good agreement between these patterns. The simulations result in an average swarm area expansion rate of 0.4 cm^2/h, which is in good agreement with the experimentally measured area expansion rate of 0.6 cm^2/h (Phase II) (see Fig. 7).

The simulated internal cell wave propagates in the radial direction with a speed of 0.24 cm/h, compared with the experimentally measured wave propagation speed of 0.08 cm/h (see Fig. 4 *A*). Thus, our model overestimates the actual cell wave propagation speed observed in our experiments. This may be due to several reasons, which

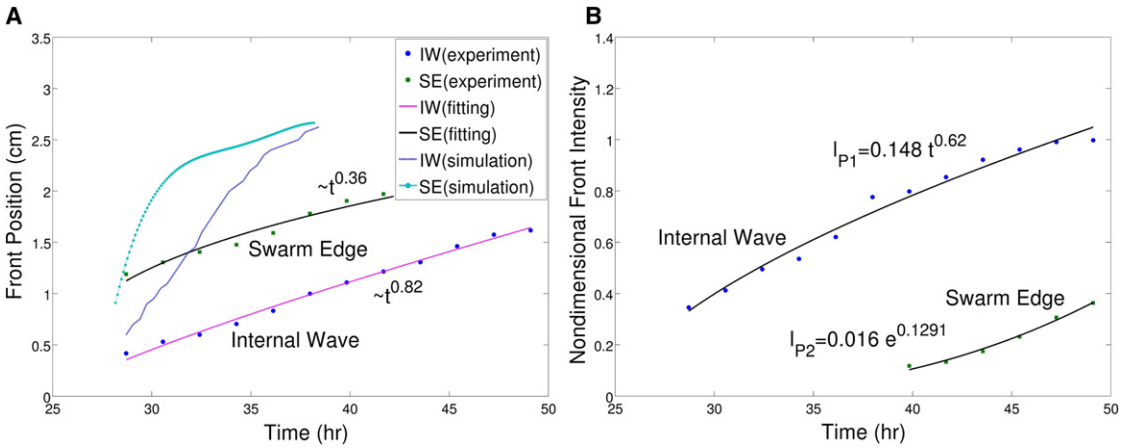

FIGURE 4 (*A*) Positions of the internal wave (IW) and of the swarm edge (SE) on soft agar as a function of time. Speeds of SE expansion are 0.05 and 0.18 cm/h in experiments (*black line*) and simulation (*light blue dashed line*), respectively. Speeds of IW propagation are 0.08 and 0.24 cm/h in experiments (*purple line*) and simulation (*dark blue line*), respectively. (*B*) Nondimensional bacterial density as a function of time. IW corresponds to the internal wave, and SE corresponds to the density near the swarm edge.

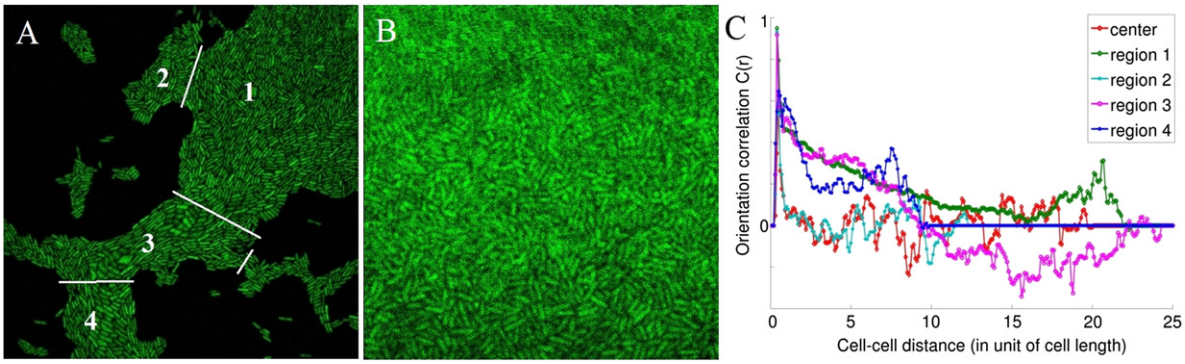

FIGURE 5 Calculation of orientation correlation of *P. aeruginosa* cells at the swarm edge and in the internal wave. Experimental images show one representative horizontal plane acquired using confocal microscopy to obtain multiple planes (in the z-direction) of green fluorescent protein-labeled cells. (*A*) Cells are closely packed and form rafts in a tendril at the swarm edge. The tendril is divided into four regions (*as marked in the figure*). Orientation correlation for each region was computed. (*B*) Patterning of cells within one plane within the cell wave. Cells also form rafts. Although cells in the wave of high cell density show certain alignment with neighboring cells, cells at some distance from each other display random orientation. (*C*) Orientation correlations for each region indicated by green-dotted, cyan-dotted, purple-dotted, and blue-dotted lines, respectively, and red-dotted line for the region of the wave of high cell density. Calculation of orientation correlations reveals that cells in the tendril show strong alignment with each other, whereas cells in the wave of high cell density display random orientation with respect to each other.

cannot currently be discerned. It is not possible to experimentally measure the actual cell division rate and RL production rate within the wave region. Moreover, it is not currently possible to experimentally discern the actual mechanism by which individual cells use specific motility modes at different locations within swarms. Finally, the effective viscosity model adopted in the work does not take into account any potential effects of cell motion on varying viscosity (27).

We also performed simulations without increasing rates of cell division and RL production and without cell alignment to study their impacts on swarming. Our simulation still showed tendril formation and produced an average swarm area expansion rate of 1.13 cm^2/h (see Figs. S1 and S2). However, these simulations did not produce propagation of high cell density and RL-dense waves. We hypothesize that the formation of these waves is likely due to increased cell division and RL production and cell alignment; this will require verification with laboratory experiments.

Finally, we compared simulations of the tendril-forming and nontendril swarms and showed that without sufficient liquid extraction and, therefore, without sufficient thickness of liquid film, swarming was extremely slow.

Scaling analysis

Both scaling analysis (37) and simulations have been used to demonstrate effects of viscosity and Marangoni forces on expanding swarms. Because it is difficult to measure viscosity of *P. aeruginosa* swarms, we adopted the viscosity value used in (27) for *Bacillus subtilis* spreading $\mu \approx 200$ *cP*. The spreading of a liquid film is assumed starting with an initial thickness H and width L ($H \ll L$). RL is assumed to be uniformly distributed within the liquid with surface and bulk concentrations Γ_m and c_m, respectively. The solid substrate is assumed to be initially coated with a liquid of uniform thickness H_b ($H_b \ll H$).

Marangoni forces are generated by the initial difference between the surface tension γ_m of the liquid with certain

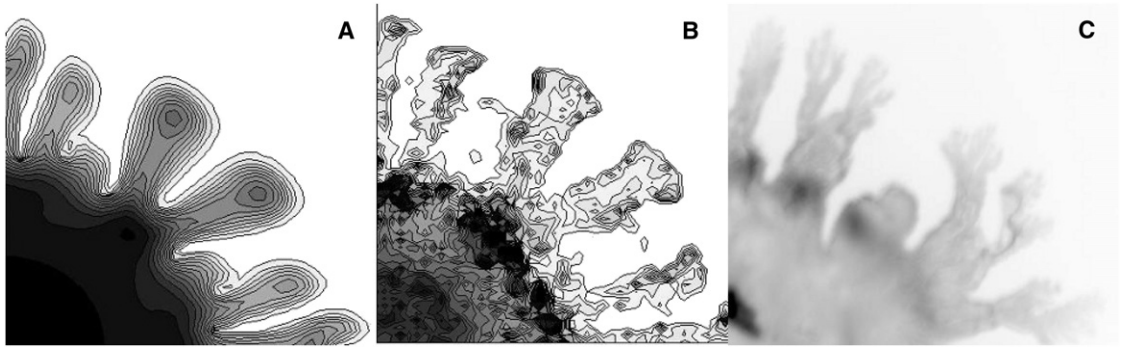

FIGURE 6 Simulation of primary and secondary tendril development. (*A*) Water height profile in a simulation at $t = 7$ h. (*B*) Cell density distribution in a simulation at $t = 7$ h. (*C*) Experimental image of a swarm on soft agar for comparison. Primary and secondary tendrils are seen to develop at the swarm edge.

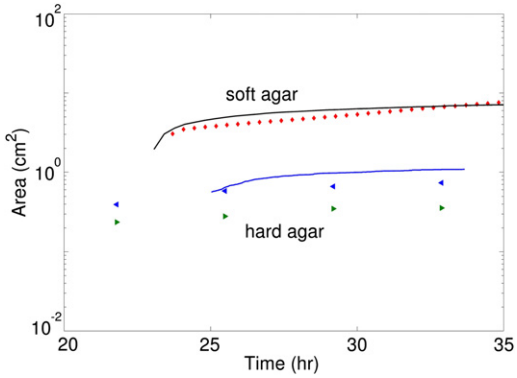

FIGURE 7 Comparison of swarm area dynamics in experiments and simulations. Black and blue lines indicate model predictions for soft and hard agar cases, respectively. Triangles represent data for swarming on hard agar plates. Experimental data for swarming on soft agar plates, represented by diamonds, agree well with the simulated data represented by a black line. Experimental data (*triangles*) and simulated data (*blue line*) also agree well with each other.

surfactant concentration, and the higher surface tension γ_c of the underlying uncontaminated film (36). We denote the maximal difference of surface tension as $S = \gamma_c - \gamma_m$. Typical experimental parameter values are $H \approx 10^{-2}$ cm, $L \approx 1$ cm, $H_b \approx 10^{-4}$ cm, $\gamma_m \approx 50$ dyn cm^{-1}, $S \approx 20$ dyn cm^{-1}, resulting in the characteristic Marangoni velocity $V = SH/(\mu L) \approx 10^{-2}$ cm/s and liquid film expanding time $T = L/V \approx 10^2$ s. The characteristic Marangoni velocity reflects a physical balance between Marangoni stresses and viscous drag. It is dependent upon the surface tension and the biofilm viscosity in a nonlinear fashion.

The finger instability observed in a surfactant deposition spreading on a thin liquid film driven by Marangoni stresses has been studied for purified surfactant (36,37). In these experiments (without bacteria), the liquid viscosity was almost the same as water, resulting in a characteristic Marangoni velocity $V \approx 40$ cm/s with fingers appearing within seconds after deposition of a surfactant droplet on an initially undisturbed thin film (see simulation results in Fig. S4 *B*). In our simulations, the viscosity of the liquid film is two orders of magnitude higher than that of water due to the suspended bacteria. This slows the finger instability response from minutes to hours, which is consistent with our experiments.

Experimental confirmation of the model prediction of cell alignment

To confirm our simulation prediction of cells being closely packed and forming aligned cells, we determined cell alignment in horizontal sections of laboratory experiment swarms.

We determined the level of cell alignment in these images using the orientation correlation function $C(r)$ introduced in (29),

$$C(r) = \frac{1}{N(r)} \sum_{i,j,i\neq j}^{N(r)} \left(2\cos^2(\theta_{ij}) - 1\right),$$

where θ_{ij} is the angle between the ith and jth cells, and $N(r)$ is the number of pairs of cells separated by a distance r (using cell length as a unit length).

Alignment of cells was determined within a tendril at the swarm edge (see Fig. 5). The green-dotted, cyan-dotted, purple-dotted, and blue-dotted lines in Fig. 5 *C* show orientation correlations for the four regions (Fig. 5 *A*), respectively. We found that for each region, absolute values of correlation $C(r) > 0.3$ for small r, i.e., nearby cells have a high probability of being aligned with each other; $C(r)$ then decreases rapidly at larger values of r. The rises of $C(r)$ at $r \approx 22$ in region 1 and $r \approx 8$ in region 4 correspond to the case that cells at the very boundary of the tendril are in parallel with the boundary of the tendril.

Within the propagating wave of the swarm, these neighboring cells are closely packed and have formed rafts (see Fig. 5 *B*). The calculated orientation correlation of the cells within the wave is shown by the red-dotted curve in Fig. 5 *C*. Oscillations of the curve indicate that cell rafts in the cell wave region mostly orientate randomly. Furthermore, orientation correlation in the high cell density wave region is much lower than that at the edge of the swarm where cell rafts mostly move in the direction of tendrils (see Fig. 5, *A* and *B*).

CONCLUSIONS

In this work, it is first shown that for the bacterium *P. aeruginosa*, cell-dense and RL-dense waves form and propagate through developing swarms from the center toward the edge of the swarm (Fig. 2). These waves result in the formation of high cell density groups within the tips of the growing tendrils at the swarm edge, creating secondary swarms. Temporal RL distribution has not been documented previously and, to our knowledge, such wave propagation has not been reported previously for swarming bacteria. This study details that the timescale at which *P. aeruginosa* is interpreting and influencing its local environment is on the order of minutes to hours; understanding of swarm dynamics is very important to fully understand bacterial swarming. We propose that this wave movement of bacteria into newly formed tendrils results in rapid and efficient colonization of new territory.

Analysis of the experiments, combined with the model simulations, suggest a mechanism of internal cell wave propagation based on increased cell division and RL production rates when cells leave the initial inoculation region, as well as increased cell-cell alignment. Our model simulations, based on these assumptions, correctly predicted the rate of *P. aeruginosa* swarm expansion and cell wave propagation speed. Simulations also showed that an increase in

cell division rate alone does not lead to wave formation in the simulations.

Shapes of the simulated tendrils are in qualitative agreement with the experimental observations (see Fig. 6, *B* and *C*). Simulations demonstrated that branched tendril formation could be governed by the changing viscosity of the bacterial liquid suspension and the liquid film boundary expansion caused by Marangoni forces. Namely, significant viscous drag resulting from the increased viscosity of the liquid film due to the presence of densely packed *P. aeruginosa* cells, resulted in reducing the liquid film's spreading speed. At the same time, *P. aeruginosa* cells produce RL, which reduces surface tension resulting in the creation of the Marangoni force due to the surface tension gradient that overcomes the viscous drag and pushes the liquid film outward.

Small perturbations at the swarm boundary get amplified due to Marangoni stresses and result in tendril formation. The *P. aeruginosa* high density cell wave efficiently and quickly propagates into these tendrils and secondary tendrils develop. Scaling analysis shows at least three orders of magnitude difference in rates of pure liquid film expansion induced by Marangoni force and *P. aeruginosa* swarm expansion. This difference is due to increased viscosity of the liquid film with cell suspension. Thus, it is critical for *P. aeruginosa* cells to produce RL and create a surface tension gradient of the liquid film in order to colonize new territory efficiently.

Tracking analysis of cells imaged using time-lapse confocal microscopy showed cells being closely packed and forming rafts of aligned cells in the propagating wave, which do not have a preferred direction of motion. Cells inside tendrils tend to swarm in the longitudinal direction. Therefore, our future research will focus on the question of how the observed cell density wave propagation is related to individual cell swarming. Our current understanding of swarming dynamics is still limited. Nevertheless, our experimental and simulation findings suggest new specific experiments to study swarming dynamics. In particular, to better understand the swarm wave dynamics, we will need to determine whether there is a difference in flagellar and pili function for cells within the waves compared to other regions.

To summarize, findings in this work detail a new strategy of efficient colonization and community development by bacteria that has not been previously documented, to our knowledge. *P. aeruginosa* uses the surfactant RL to control physical forces needed by swarms to efficiently expand over surfaces as a thin liquid film. Although it is well known that biological organisms respond to environmental cues, these swarming bacteria respond actively to alter their environment on a short timescale to greatly improve their colonization rate.

SUPPORTING MATERIAL

Six figures, a table, six movies, and references are available at http://www.biophysj.org/biophysj/supplemental/S0006-3495(12)00724-2.

We thank Cameron Harvey for the helpful discussions, Xiaomin Liu for the help with image analysis, and Catherine Stecyk for assistance with the time-lapse microscopy.

We acknowledge partial support from the National Institutes of Health grants NIH 1 R01 GM100470-01 and NIH 1 R01GM095959-01A1 (H.D., Z.X., J.D.S., and M.A.), National Science Foundation grants DMS-0800612, DMS-1115887 and DMS-0719895 (H.D., Z.X., and M.A.), and the Indiana Clinical and Translational Science Institute (NIH No. UL1RR025761) (J.D.S.).

REFERENCES

1. Caiazza, N. C., J. H. Merritt, …, G. A. O'Toole. 2007. Inverse regulation of biofilm formation and swarming motility by *Pseudomonas aeruginosa* PA14. *J. Bacteriol.* 189:3603–3612.
2. Overhage, J., S. Lewenza, …, R. E. Hancock. 2007. Identification of genes involved in swarming motility using a *Pseudomonas aeruginosa* PAO1 mini-Tn5-*lux* mutant library. *J. Bacteriol.* 189:2164–2169.
3. Shrout, J. D., D. L. Chopp, …, M. R. Parsek. 2006. The impact of quorum sensing and swarming motility on *Pseudomonas aeruginosa* biofilm formation is nutritionally conditional. *Mol. Microbiol.* 62:1264–1277.
4. Henrichsen, J. 1972. Bacterial surface translocation: a survey and a classification. *Bacteriol. Rev.* 36:478–503.
5. Jarrell, K. F., and M. J. McBride. 2008. The surprisingly diverse ways that prokaryotes move. *Nat. Rev. Microbiol.* 6:466–476.
6. Kearns, D. B. 2010. A field guide to bacterial swarming motility. *Nat. Rev. Microbiol.* 8:634–644.
7. Venturi, V., I. Bertani, …, S. Pongor. 2010. Co-swarming and local collapse: quorum sensing conveys resilience to bacterial communities by localizing cheater mutants in *Pseudomonas aeruginosa*. *PLoS ONE.* 5:e9998.
8. Xavier, J. B., W. Kim, and K. R. Foster. 2011. A molecular mechanism that stabilizes cooperative secretions in *Pseudomonas aeruginosa*. *Mol. Microbiol.* 79:166–179.
9. Darnton, N. C., L. Turner, …, H. C. Berg. 2010. Dynamics of bacterial swarming. *Biophys. J.* 98:2082–2090.
10. Ingham, C. J., and E. Ben Jacob. 2008. Swarming and complex pattern formation in *Paenibacillus vortex* studied by imaging and tracking cells. *BMC Microbiol.* 8:36.
11. Turner, L., R. Zhang, …, H. C. Berg. 2010. Visualization of flagella during bacterial swarming. *J. Bacteriol.* 192:3259–3267.
12. Zhang, H. P., A. Be'er, …, H. L. Swinney. 2009. Swarming dynamics in bacterial colonies. *EPL.* 87:48011.
13. Zhang, R., L. Turner, and H. C. Berg. 2010. The upper surface of an *Escherichia coli* swarm is stationary. *Proc. Natl. Acad. Sci. USA.* 107:288–290.
14. Wu, Y., B. G. Hosu, and H. C. Berg. 2011. Microbubbles reveal chiral fluid flows in bacterial swarms. *Proc. Natl. Acad. Sci. USA.* 108:4147–4151.
15. Shigematsu, M., Y. Meno, …, K. Amako. 1995. The measurement of swimming velocity of *Vibrio cholerae* and *Pseudomonas aeruginosa* using the video tracking methods. *Microbiol. Immunol.* 39:741–744.
16. Mattick, J. S. 2002. Type IV pili and twitching motility. *Annu. Rev. Microbiol.* 56:289–314.
17. Murray, T. S., and B. I. Kazmierczak. 2008. *Pseudomonas aeruginosa* exhibits sliding motility in the absence of type IV pili and flagella. *J. Bacteriol.* 190:2700–2708.
18. O'Toole, G. A., and R. Kolter. 1998. Flagellar and twitching motility are necessary for *Pseudomonas aeruginosa* biofilm development. *Mol. Microbiol.* 30:295–304.
19. Gibiansky, M. L., J. C. Conrad, …, G. C. Wong. 2010. Bacteria use type IV pili to walk upright and detach from surfaces. *Science.* 330:197.

20. Kamatkar, N. G., and J. D. Shrout. 2011. Surface hardness impairment of quorum sensing and swarming for *Pseudomonas aeruginosa*. *PLoS ONE.* 6:e20888.

21. Caiazza, N. C., R. M. Shanks, and G. A. O'Toole. 2005. Rhamnolipids modulate swarming motility patterns of *Pseudomonas aeruginosa*. *J. Bacteriol.* 187:7351–7361.

22. Köhler, T., L. K. Curty, …, J. C. Pechère. 2000. Swarming of *Pseudomonas aeruginosa* is dependent on cell-to-cell signaling and requires flagella and pili. *J. Bacteriol.* 182:5990–5996.

23. Ochsner, U. A., and J. Reiser. 1995. Autoinducer-mediated regulation of rhamnolipid biosurfactant synthesis in *Pseudomonas aeruginosa*. *Proc. Natl. Acad. Sci. USA.* 92:6424–6428.

24. Pearson, J. P., E. C. Pesci, and B. H. Iglewski. 1997. Roles of *Pseudomonas aeruginosa las* and *rhl* quorum-sensing systems in control of elastase and rhamnolipid biosynthesis genes. *J. Bacteriol.* 179:5756–5767.

25. Bees, M. A., P. Andresén, …, M. Givskov. 2000. The interaction of thin-film flow, bacterial swarming and cell differentiation in colonies of *Serratia liquefaciens*. *J. Math. Biol.* 40:27–63.

26. Bees, M. A., P. Andresén, …, M. Givskov. 2002. Quantitative effects of medium hardness and nutrient availability on the swarming motility of *Serratia liquefaciens*. *Bull. Math. Biol.* 64:565–587.

27. Angelini, T. E., M. Roper, …, M. P. Brenner. 2009. *Bacillus subtilis* spreads by surfing on waves of surfactant. *Proc. Natl. Acad. Sci. USA.* 106:18109–18113.

28. Wu, Y., Y. Jiang, …, M. Alber. 2007. Social interactions in myxobacterial swarming. *PLoS Comput. Biol.* 3:e253.

29. Wu, Y. L., A. D. Kaiser, …, M. S. Alber. 2009. Periodic reversal of direction allows Myxobacteria to swarm. *Proc. Natl. Acad. Sci. USA.* 106:1222–1227.

30. Harvey, C. W., F. Morcos, …, M. Alber. 2011. Study of elastic collisions of *Myxococcus xanthus* in swarms. *Phys. Biol.* 8:026016.

31. Du, H. J., Z. L. Xu, …, M. Alber. 2011. Multiscale modeling of *Pseudomonas aeruginosa* swarming. *Math Models Methods Appl. Sci.* 21 (*Suppl 1*):939–954.

32. Craster, R. V., and O. K. Matar. 2009. Dynamics and stability of thin liquid films. *Rev. Mod. Phys.* 81:1131–1198.

33. Matar, O. K., and S. M. Troian. 1997. Linear stability analysis of an insoluble surfactant monolayer spreading on a thin liquid film. *Phys. Fluids.* 9:3645–3657.

34. Sheludko, A. 1967. Thin liquid films. *Adv. Colloid Interface Sci.* 1:391–464.

35. Warner, M. R. E., R. V. Craster, and O. K. Matar. 2002. Unstable van der Waals driven line rupture in Marangoni driven thin viscous films. *Phys. Fluids.* 14:1642–1654.

36. Warner, M. R. E., R. V. Craster, and O. K. Matar. 2004. Fingering phenomena created by a soluble surfactant deposition on a thin liquid film. *Phys. Fluids.* 16:2933–2951.

37. Warner, M. R. E., R. V. Craster, and O. K. Matar. 2004. Fingering phenomena associated with insoluble surfactant spreading on thin liquid films. *J. Fluid Mech.* 510:169–200.

38. Morris, J. D., J. L. Hewitt, …, J. D. Shrout. 2011. Imaging and analysis of *Pseudomonas aeruginosa* swarming and rhamnolipid production. *Appl. Environ. Microbiol.* 77:8310–8317.

39. Newman, M. E. J., and G. T. Barkema. 1999. Monte Carlo Methods in Statistical Physics. Clarendon Press; Oxford University Press, Oxford.

40. Netotea, S., I. Bertani, …, S. Pongor. 2009. A simple model for the early events of quorum sensing in *Pseudomonas aeruginosa*: modeling bacterial swarming as the movement of an "activation zone". *Biol. Direct.* 4:6.

41. Dockery, J. D., and J. P. Keener. 2001. A mathematical model for quorum sensing in *Pseudomonas aeruginosa*. *Bull. Math. Biol.* 63:95–116.

42. Melke, P., P. Sahlin, …, H. Jönsson. 2010. A cell-based model for quorum sensing in heterogeneous bacterial colonies. *PLoS Comput. Biol.* 6:e1000819.

43. Craster, R. V., and O. K. Matar. 2006. Numerical simulations of fingering instabilities in surfactant-driven thin films. *Phys. Fluids.* 18:032103–032112.

44. Verberg, R., I. M. de Schepper, and E. G. D. Cohen. 1997. Viscosity of colloidal suspensions. *Phys. Rev. E.* 55:3143–3158.

45. Dussaud, A. D., O. K. Matar, and S. M. Troian. 2005. Spreading characteristics of an insoluble surfactant film on a thin liquid layer: comparison between theory and experiment. *J. Fluid Mech.* 544:23–51.

46. Fallest, D. W., A. M. Lichtenberger, …, K. E. Daniels. 2010. Fluorescent visualization of a spreading surfactant. *New J. Phys.* 12:073029.

47. Marmur, A. 2004. The Lotus effect: superhydrophobicity and metastability. *Langmuir.* 20:3517–3519.

48. Chen, B. G., L. Turner, and H. C. Berg. 2007. The wetting agent required for swarming in *Salmonella enterica* serovar typhimurium is not a surfactant. *J. Bacteriol.* 189:8750–8753.

49. Be'er, A., R. S. Smith, …, H. L. Swinney. 2009. *Paenibacillus dendritiformis* bacterial colony growth depends on surfactant but not on bacterial motion. *J. Bacteriol.* 191:5758–5764.

50. Ben-Jacob, E., I. Cohen, …, L. Tsimring. 1995. Complex bacterial patterns. *Nature.* 373:566–567.

51. Berg, H. C. 2005. Swarming motility: it better be wet. *Curr. Biol.* 15:R599–R600.

52. Harshey, R. M. 2003. Bacterial motility on a surface: many ways to a common goal. *Annu. Rev. Microbiol.* 57:249–273.